Jovian Capture of a Spacecraft with a Self-Balanced Electrodynamic Bare Tether

M. Sanjurjo-Rivo*
Universidad Carlos III, Leganés, 28911 Madrid, Spain
D. J. Scheeres†
University of Colorado at Boulder, Boulder, Colorado 80309
and
J. Peláez‡
Universidad Politécnica de Madrid, 28040 Madrid, Spain

This paper proposes and analyzes the use of a nonrotating tethered system for a direct capture in Jovian orbit using the electrodynamic force generated along the cable. A detailed dynamical model is developed showing a strong gravitational and electrodynamic coupling between the center of mass and the attitude motions. This paper shows the feasibility of a direct capture in Jovian orbit of a rigid tethered system preventing the tether from rotating. Additional mechanical–thermal requirements are explored, and preliminary operational limits are defined to complete the maneuver. In particular, to ensure that the system remains nonrotating, a nominal attitude profile for a self-balanced electrodynamic tether is proposed, as well as a simple feedback control.

Nomenclature

$\boldsymbol{B}$	=	magnetic field, T
d_t	=	width of the tether, m
E_m	=	motional electric field projected in the tether direction, V/m
$\boldsymbol{E}_m$	=	motional electric field, V/m
e	=	modulus of osculating eccentricity of the trajectory
$\boldsymbol{e}$	=	osculating eccentricity vector
e_c	=	electron charge, C
$\boldsymbol{F}_{\text{ed}}$	=	total electrodynamic force on tether, N
$\boldsymbol{F}_{\text{ed}}^{ds}$	=	electrodynamic force on tether element, N
$\boldsymbol{F}_P$	=	perturbation force, N
$\mathcal{F}_{I_s}$	=	nondimensional function
$\mathcal{G}$	=	nondimensional function
h	=	modulus of specific angular momentum of the trajectory, m^2/s
$\boldsymbol{h}$	=	specific angular momentum of the trajectory, m^2/s
h_0	=	initial modulus of the specific angular momentum, m^2/s^{-1}
$\hat{h}$	=	nondimensional specific angular momentum
h_t	=	thickness of the tether, m
I	=	current along the tether, A
I_{av}	=	averaged current along the tether, A
$\bar{I}_G$	=	inertia tensor of the tethered system, $\text{kg} \cdot \text{m}^2$
I_{m1}	=	dimensional first momentum of the current profile, $\text{A} \cdot \text{m}$
I_{OML}	=	current on the orbital motion-limited regime, A
I_s	=	moment of inertia perpendicular to tether direction, $\text{kg} \cdot \text{m}^2$
i_{av}	=	nondimensional averaged current along the tether
i_{m1}	=	nondimensional first momentum of the current profile
$\boldsymbol{L}_G$	=	angular momentum with respect to the center of mass, $\text{kg} \cdot \text{m}^2/\text{s}$
L_t	=	tether length, m
ℓ_t	=	nondimensional tether length
$\boldsymbol{M}$	=	torques on the center of mass, $\text{N} \cdot \text{m}$
$\boldsymbol{M}_{\text{ed}}$	=	electrodynamic torque on the center of mass, $\text{N} \cdot \text{m}$
M_{gg}	=	gravitational torque on the center of mass, $\text{N} \cdot \text{m}$
m	=	total mass of the tethered system, kg
m_1	=	lower mass, kg
m_2	=	upper mass, kg
m_e	=	electron mass, kg
m_t	=	tether mass, kg
n_∞	=	electron plasma density, $1/\text{m}^3$
$\mathcal{P}_i$	=	nondimensional functions
p_t	=	tether perimeter, m
$\boldsymbol{q}$	=	inertial orientation of tether element
R_J	=	Jupiter equatorial radius, m
$\boldsymbol{r}$	=	position vector of tether mass element, m
$\boldsymbol{r}_G$	=	position vector of the center of mass of the tethered system, m
r_p	=	radius of perijove of initial hyperbolic orbit, m
s	=	arc length of the tether, m
t	=	time, s
$\boldsymbol{u}$	=	direction of unit vector from cathode to anode
$\boldsymbol{u}_r$	=	unit vector along radial direction
$\boldsymbol{u}_\theta$	=	unit vector along transversal direction
$\boldsymbol{v}$	=	inertial velocity of tether element, m/s
$\boldsymbol{v}^{\text{rel}}$	=	relative velocity between tether and plasma, m/s
$\boldsymbol{v}_{\text{pl}}$	=	plasma inertial velocity, m/s
$\boldsymbol{v}_{\text{SC}}$	=	spacecraft inertial velocity, m/s
v_∞	=	arrival velocity at Jupiter, m/s
α	=	longitude of periapsis, rad
Γ	=	ratio tether to total mass of the system
γ	=	ratio between two characteristic times
θ	=	true anomaly, rad
κ	=	nondimensional parameter
Λ	=	nondimensional parameter
μ	=	electron-to-ion-mass ratio
μ_m	=	dipole field strength, T
μ_J	=	Jupiter gravitational constant, m^3/s^2
ρ_v	=	volumetric density of the tether, kg/m^3
σ_c	=	conductivity of the tether, $1/(\Omega \cdot \text{m})$
τ	=	nondimensional time

Presented at the 19th AAS/AIAA Space Flight Mechanics Meeting, Savannah, GA, 9–12 February 2009; received 22 November 2012; revision received 13 May 2013; accepted for publication 14 May 2013; published online 21 February 2014.

*Visiting Professor, Bioengineering and Aerospace Department; manuel.sanjurjo@uc3m.es.
†Professor, Seebass Chair, Aerospace Engineering.
‡Professor, E.T.S.I. Aeronáuticos, Applied Physics. Member AIAA.

τ_c = characteristic time, s
Φ_p = tether plasma bias, V
ϕ = angle between tether direction and radial direction, rad
χ = mass angle (describes mass distribution), rad
ψ = angle between tether direction and inertial x axis, rad
Ω = angular velocity of the siderial rotation of Jupiter, 1/s
Ω_t = nondimensional electric load
Ω_0 = volume of the tethered system, m^3
ω = angular velocity of the tethered system, 1/s

I. Introduction

THE exploration of Jupiter and the Jovian system is a current priority for planetary scientists and space agencies. Increasing our knowledge on the Jovian system would help to understand the Solar System formation and the behavior of similar planets in extrasolar systems as well as to assess the habitability of its moons (Europa in particular) [1]. The exploration of Jupiter, however, also constitutes an engineering challenge. Missions to the outer planets have to face two important limitations that constrain their operability and their scientific payload: on one hand, the necessary propellant mass for the capture, and on the other hand, the scarcity of power generation. Both of these have had an important impact on the design of previous missions to Jupiter. The search for solutions to avoid these handicaps led to the proposal of the Jupiter Icy Moons Orbiter (JIMO) mission, which enhanced the performance compared to former missions. JIMO would have used a small nuclear reactor to overcome the weak electrical power generation and to power ion electric thrusters, improving mission maneuvering.

In this scenario, electrodynamic tethers can represent a suitable solution because they can address both limitations simultaneously. Moreover, they can also be used to study the Jovian magnetosphere. A complete and thorough analysis of a tether mission to Jupiter is presented in Sanmartin et al. [2–4] and Charro et al. [5]. There are also a number of works that explore the advantages of electrodynamic tethers in the Jovian system to produce power. In Peláez and Scheeres [6,7], a new strategy to provide power in a permanent manner using electrodynamic tethers is fully described and analyzed for a Jovian orbit; in Bombardelli et al. [8], an electrodynamic tether system to produce power keeping the orbital energy unaltered is presented; and finally, in Curreli et al. [9], the power generation in the Jovian torus with an electrodynamic tether is analyzed, highlighting the advantages of the system. Related to the use of electrodynamic tethers in Jovian orbit, the possibility of using them as a primary propulsive system for the capture maneuver in Jupiter has been explored. In fact, the problem of using electrodynamic tethers to perform the capture maneuver has been studied in several articles. Gallagher et al. [10] presents a numerical computation of spacecraft trajectories assuming a given attitude for the tether and an ad hoc model of the current collection. Besides, they consider retrograde captures and provide a study of the possible thermal side effects on the cable. In turn, Sanmartin and Lorenzini [11] give a fully analytical estimation of an electrodynamic tether's performance and the main parameters involved in a prograde capture with an accurate model of the current collection as well as some simplifications concerning the geometry of the trajectory and the attitude of the tether. In this work, the concept of the drag sphere was presented, inside of which the tether produces drag and outside of which it can generate thrust. In van Dijk et al. [12], a complete study of the electrodynamic force capabilities of electrodynamic tethers in the Jovian environment is developed. The attitude is considered here in detail, though the results are applied only to circular orbits. Finally, Sanmartin et al. [2,3] analyze the performance of rapidly rotating tethers in the capture maneuver and study their operative limits due to excessive heating or bowing. Rapidly rotating tethers succeed in addressing the operational constraints of the capture maneuver. Nevertheless, many of the proposals to operate an electrodynamic tether in Jovian orbit require the tether to be nonrotating. Therefore, the possibility of completing the Jovian capture maneuver with an SBET could reduce the complexity of the mission and the delta-V budget.

The aim of this paper is the analysis of the attitude dynamics of an electrodynamic tether in a capture maneuver and the capability to control the orientation of the tether with the electrodynamic forces alone. To achieve that goal, a comprehensive dynamical model is derived, gathering the relevance of the attitude dynamics in the capture as well as keeping the accuracy of the environmental models. The proposed capture method is based on the self-balanced electrodynamic tether (SBET) concept [13] to prevent the tether from rotating after the capture. The main characteristic of SBETs is that they avoid the instabilities associated with the attitude dynamics in inclined orbits. In the near-Earth environment, SBETs have proven their capability to stabilize electrodynamic tethers [14], combining high tether intensities with no perturbation torques and therefore with a stable attitude state. This property allows the tether to work aligned with the local vertical, which represents an important benefit in terms of current collection efficiency in addition to the desired attitude stability. In other words, the eletric power developed during the capture is enhanced by using a SBET. The consideration of the former criterion leads to the use of tethers without insulation, called bare tethers, given that this solution solves the problem of anodic contact in highly rarefied plasma [15]. In addition, the feasibility of using rigid nonrotating electrodynamic tethers to perform a direct Jovian capture maneuver is assessed in a broader sense, making rough estimations of the operational limits due to thermal and mechanical effects.

The next section is devoted to describing the maneuver and the tethered system, comparing the models used with those applied in previous studies. The following sections are aimed to define in detail the complete dynamical model that is used in the analysis of the Jovian capture. Then, the control options of nonrotating tethers are explored in detail, arriving at the establishment of a control strategy. Last, a thermal analysis of the cable has been performed, following the previous analysis in Sanmartin et al. [3]. The high currents that the tether would provide produce the heating of the cable due mainly to ohmic effects. This element can be a limiting factor of the allowable current that can be borne. Considering this fact, the operational limits for nonrotating tethers are established.

II. Description of the Tether Maneuver

The electrodynamic tether generates drag only in a fraction of an arc of the whole trajectory. Because of this, the tethered system will follow a hyperbolic trajectory during the first part of the maneuver, within the validity of the patched conic approximation. This initial hyperbolic orbit can be defined completely by means of the arrival velocity $\boldsymbol{v}_\infty$, the radius of the periapsis, $\boldsymbol{r}_p$, and the orbital plane (by definition of the Jovian reference frame, $\omega + \Omega = 0$). All of the foregoing studies, as well as the present, have considered an equatorial plane for the capture maneuver because it represents the most effective solution in terms of the electrodynamic work that can be provided. Additionally, the initial relative velocities that have been considered vary from 5.64 km/s of the minimum-energy transfer from the Earth (ignoring the inclination of Jupiter's orbit with respect to the ecliptic) in Sanmartin et al. [2] to 6 km/s in Sanmartin and Lorenzini [11] and to 6.854 km/s of a previous concept space mission in Gallagher et al. [10]. In this article, we will consider arrival velocities of 1.0 and 1.2 times the velocity of the Hohmann transfer. On the other hand, the considered radius of periapsis varies from 1.01 R_J (from a proposed mission Radio Science Observer) in Gallagher et al. [10] to 1.5 R_J in Sanmartin and Lorenzini [11]. In retrograde capture orbits, there are no constraints on this parameter, but in prograde orbit, it is necessary that the perijove is inside the drag sphere (generally speaking, because for hyperbolic orbits, the stationary radius is not well-defined). From the results of these articles, it can be deduced that the radius of periapsis is a decisive parameter in the design of Jovian capture trajectories. In the current work, we will explore the results obtained for the radius of periapsis between 1.0 R_J and 2.0 R_J.

Regarding the computation of electrodynamic forces, it is necessary to establish a model for current collection. The interaction among a conductive tether, the ionosphere, and magnetic field of a

planet like Jupiter can lead to the generation of a current inside the cable. In a frame orbiting with the tether, there exists an electric field given by

$$\boldsymbol{E}_m = (\boldsymbol{v}_{\mathrm{SC}} - \boldsymbol{v}_{\mathrm{pl}}) \times \boldsymbol{B} \tag{1}$$

where $\boldsymbol{v}_{\mathrm{SC}}$ and $\boldsymbol{v}_{\mathrm{pl}}$ are the inertial velocities of the spacecraft and the plasma, respectively. This field can drive a current inside the tether. The study of the mechanisms that determine the tether current collection is out of the scope of this analysis. Still, it should be clarified that the current through the cable will be different as a function of the anodic contactors used. There are basically two procedures to collect electrons: a balloon at the anodic end of the tether, where the collection follows the Parkers–Murphy current, or a bare tether [2,11,12], where the collection takes place in the orbital motion-limited (OML) regime, as long as some conditions regarding the transversal tether dimensions are fulfilled. In Gallagher et al. [10], a combination of both is considered. The bare tether has been chosen as the preferable option, as it has been discussed before.

In the OML regime, the evolution of the current along the tether is governed by the following equation [16]:

$$I_{\mathrm{OML}} = L_t n_\infty e_c \frac{p_t}{\pi} \sqrt{\frac{2 e_c \Phi_p}{m_e}} \tag{2}$$

where p_t is the tether perimeter, n_∞ is the electron plasma density, e_c is electron charge, m_e is the electron mass, and Φ_p is the tether plasma bias. Therefore, current collection depends on the differential potential between the cable and the surrounding plasma, and hence it is necessary to compute its evolution considering the motional electric field along the cable, E_m, and the ohmic losses due to the current. The statement of the full set of differential equations that model the current collection is presented in Sanmartin and Ahedo [15] and Martinez-Sanchez and Sanmartin [17]. The statement of this problem is completed with boundary conditions at both ends where a hypothetical load for power generation and the voltage drop at the cathodic end appear. As a result, a system of differential equations with boundary conditions must be solved to obtain the current and bias profile along the cable.

Regarding the environment of Jupiter, the magnetic field is generally considered as a no-tilt dipole [2,12] whose characteristics are described in Divine and Garret [18]. Nevertheless, in Gallagher et al. [10], a more complex model [19] is followed. On the other hand, to determine the charge population, the work of Divine and Garret [18] is generally used. Still, in Gallagher et al. [10], a simplified version of a more extended model [20] has been considered. For a deep discussion about the Jovian environmental conditions related to the operation of electrodynamic tethers, see Sanmartin et al. [2].

The dumbbell model will be used to describe the tethered system. This model allows us to provide a first approximation of the system behavior. The tether is supposed to be a conductive rod with mass m_t and length L_t, connecting two end masses m_1 (the lower mass) and m_2 (the upper mass). Instead of m_1, m_2, and m_t, the parameters m, the total mass, χ, and Γ have been used to describe the configuration of mass. Their definitions are as follows:

$$m = m_1 + m_2 + m_t \qquad m_t = m\Gamma \tag{3}$$

$$m_1 = m\left(\cos^2(\chi) - \frac{\Gamma}{2}\right) \qquad m_2 = m\left(\sin^2(\chi) - \frac{\Gamma}{2}\right) \tag{4}$$

The maximum and minimum values of χ are reached when $m_1 = 0$ and $m_2 = 0$, respectively. Then, χ is defined in the interval $[\chi_{\min}, \chi_{\max}]$ whose values are given by

$$\chi_{\min} = \arcsin\left(\frac{\Gamma}{2}\right) \qquad \chi_{\max} = \arccos\left(\frac{\Gamma}{2}\right) \tag{5}$$

In turn, the value of the moments of inertia with respect to the direction of the cable is assumed to be zero. For any other perpendicular direction, the value of the moment of inertia is I_s. Expressed in terms of the parameters of the geometry of mass, I_s is equal to

$$I_s = \frac{1}{12} m_t L_t^2 (3\sin^2(2\chi) - 2\Gamma) \tag{6}$$

The more restrictive assumption of the dumbbell model for the case of study is the hypothesis that the tether remains straight. Tethers relay on gravity gradient to produce passively the required tension to remain straight. The combination of a weak gravity gradient in Jupiter and high lateral forces makes a nonrotating tether unable to generate passively the required tension. Nevertheless, the required tension could be supplied actively with actuators on the tether ends.

III. Motion of the Center of Mass

In this section, a description of the dynamics of the center of mass is derived in terms of the osculating orbital elements of the trajectory. This characterization allows us to provide further insight on the maneuver as well as to develop an easy numerical implementation.

Before exposing the detailed derivation of the dynamical equations, it is necessary to present the model used for the electrodynamic force acting upon the tether. The electrodynamic force that appears on a tether element, $\boldsymbol{F}_{\mathrm{ed}}^{ds}$, can be computed as

$$\boldsymbol{F}_{\mathrm{ed}}^{ds} = I(s, \boldsymbol{r}, \boldsymbol{v}, \boldsymbol{q}, \dot{\boldsymbol{q}}) \boldsymbol{u}(\boldsymbol{q}) \times \boldsymbol{B}(s, \boldsymbol{r}) \tag{7}$$

where $I(s, \boldsymbol{r}, \boldsymbol{v}, \boldsymbol{q}, \dot{\boldsymbol{q}})$ is the current along the tether, $\boldsymbol{B}(s, \boldsymbol{r})$ is the magnetic field at the tether element, $\boldsymbol{u}(\boldsymbol{q})$ represents the unit vector in the direction from the cathode to the anode, s is the variable along the tether, and $\boldsymbol{r}, \boldsymbol{v}, \boldsymbol{q}, \dot{\boldsymbol{q}}$ is the state of the system ($\boldsymbol{q}$ and $\dot{\boldsymbol{q}}$ stand for the variables used to represent the attitude of the tether). To simplify that expression, some hypothesis are made.

1) Both the magnetic field and the velocity do not vary along the tether: $\boldsymbol{B}(s, \boldsymbol{r}) \approx \boldsymbol{B}(\boldsymbol{r})$, $\boldsymbol{v}(s, \boldsymbol{r}) \approx \boldsymbol{v}(\boldsymbol{r})$.

2) The trajectory takes place in the equatorial plane, and the tether motion is contained in this plane. Therefore, $\boldsymbol{u}$ is a function only of an angle ϕ. Expressed in cylindrical coordinates: $\boldsymbol{u} = \cos\phi \boldsymbol{u}_r + \sin\phi \boldsymbol{u}_\theta$. A scheme of the angles involved in the analysis can be seen in Fig. 1.

3) The current along the tether is computed as the average in a given instant: $L_t I_{\mathrm{av}}(\boldsymbol{r}, \boldsymbol{v}, \phi) = \int_{s_0}^{s_f} I(\xi, \boldsymbol{r}, \boldsymbol{v}, \phi)\, \mathrm{d}\xi$.

4) The magnetic field is a nontitled dipole: $\boldsymbol{B}(\boldsymbol{r}) = B(r)\boldsymbol{u}_z$. The value of $B(r)$ in Jupiter will be negative, due to the dipole orientation. Nevertheless, as it will be showed later, the electrodynamic force is proportional to $B(r)^2$, and its sign only changes the direction of the current along the tether.

Hence, the Lorentz force is written as

$$\boldsymbol{F}_{\mathrm{ed}} = L_t B(r) I_{\mathrm{av}}(\boldsymbol{r}, \boldsymbol{v}, \phi) \cdot (-\cos\phi \boldsymbol{u}_\theta + \sin\phi \boldsymbol{u}_r) \tag{8}$$

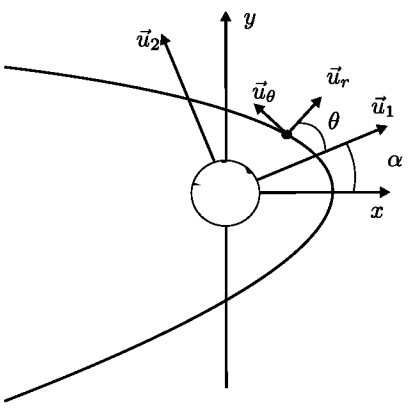

Fig. 1 Angles and vectors considered in the Jovian capture.

The averaged current along the tether can be modeled as a function of the state of the system using the OML regime model as it is presented in Sanmartin et al. [2]. According to this model,

$$I_{\text{av}}(\boldsymbol{r}, \boldsymbol{v}, \phi) = \sigma_c E_m(\boldsymbol{r}, \boldsymbol{v}, \phi) d_t h_t i_{\text{av}}(\ell_t(\boldsymbol{r}, \boldsymbol{v}, \phi), \Omega_t) \tag{9}$$

where σ_c is the conductivity of the tether material, d_t and h_t are the width and the thickness of the tape, respectively, and i_{av} is a function of ℓ_t, which is a nondimensional value proportional to the tether length, and Ω_t, which is a nondimensional value proportional to the electric load of the tether. The latter parameter is free and can be used as a control variable. In turn, E_m is the motional electrical field projected on the tether direction, and its value is computed as

$$\begin{aligned} E_m(\boldsymbol{r}, \boldsymbol{v}, \phi) &= \boldsymbol{u} \cdot [(\boldsymbol{v} - \boldsymbol{v}_{\text{pl}}) \times \boldsymbol{B}] = \boldsymbol{u} \cdot [\boldsymbol{v}^{\text{rel}} \times \boldsymbol{B}] \\ &= B(r)(v_\theta^{\text{rel}} \cos\phi - v_r^{\text{rel}} \sin\phi) \end{aligned} \tag{10}$$

Imposing the dipole moment description of the magnetic field: $B(r) = -\mu_m (R_J/r)^3$, the final result for the electrodynamic force as a function of the position, velocity, and the angle ϕ ($m_t = d_t h_t L_t/\rho_v$, tether mass) is

$$\begin{aligned} \boldsymbol{F}_{\text{ed}}(\boldsymbol{r}, \boldsymbol{v}, \phi) = &\frac{\sigma_c m_t}{\rho_v} \mu_m^2 R_J^6 \cdot \frac{i_{\text{av}}}{r^6} \cdot (v_\theta^{\text{rel}} \cos\phi - v_r^{\text{rel}} \sin\phi) \\ &\cdot (-\cos\phi \boldsymbol{u}_\theta + \sin\phi \boldsymbol{u}_r) \end{aligned} \tag{11}$$

Nevertheless, we are interested in expressing the dynamics in terms of the osculating orbital elements. Moreover, the description must be valid for all of the conics because the initial trajectory is a hyperbola and the final target trajectory is an ellipse. The radial and longitudinal velocity as well as the radius of all conics can be described as a function of the osculating orbit elements as follows:

$$\boldsymbol{v} = \frac{e\mu_J}{h} \sin\theta \quad \boldsymbol{u}_r + \frac{\mu_J}{h}(1 + e\cos\theta)\boldsymbol{u}_\theta \tag{12}$$

$$r = \frac{h^2}{\mu_J(1 + e\cos\theta)} \tag{13}$$

where e is the eccentricity, θ is the true anomaly, and h is the specific angular momentum. For convenience, the specific angular momentum will be considered instead of the semimajor axis hereafter. Furthermore, if we take into account that the velocity of the plasma is $\boldsymbol{v}_{\text{pl}} = r\Omega\boldsymbol{u}_\theta$ (for prograde trajectories), where Ω is the angular velocity of the sideral rotation of Jupiter, then the final expression for the electrodynamic force acting on the tether is

$$\boldsymbol{F}_{\text{ed}} = \Lambda i_{\text{av}} \frac{\mathcal{P}_1(1 + e\cos\theta)^6}{h^{13}} (-\cos\phi \boldsymbol{u}_\theta + \sin\phi \boldsymbol{u}_r) \tag{14}$$

where

$$\Lambda = \frac{m_t \mu_J^7 \sigma_c}{\rho_v} \mu_m^2 R_J^6 \quad \text{and}$$

$$\mathcal{P}_1(\theta, h, \phi, e) = \cos\phi + e\cos(\theta + \phi) - \frac{\Omega h^3 \cos\phi}{\mu_J^2(1 + e\cos\theta)} \tag{15}$$

A. Dynamics

The tether is considered to be rigid; therefore, we should analyze the motion of a rigid body with respect to a inertial frame $Jx_1y_1z_1$. Let $\boldsymbol{r}_G = \boldsymbol{r}_G(t)$ be the position vector of the center of mass of the tether in the inertial reference frame $Jx_1y_1z_1$. Hence, the equations of motion can be expressed as

$$m\ddot{\boldsymbol{r}}_G = -\frac{m\mu_J}{|r_G|^3} \boldsymbol{r}_G + \boldsymbol{F}_p \tag{16}$$

where $\boldsymbol{F}_p$ is the perturbation force, defined as the resultant of all the external forces acting in the system except for the main term of the gravitational potential. We will consider the electrodynamic force as the only perturbation force $\boldsymbol{F}_p = \boldsymbol{F}_{ed}$. Under the assumptions enumerated in the previous paragraph, the Lorentz force has the form gathered in Eq. (14). This constitutes a system of fourth order. The numerical integration of this system would provide us with the evolution of $\boldsymbol{r}_G(t)$ given the functions Λ and $\phi(t)$ and certain initial conditions. It can be noted that the attitude of the tether and the motion of the center of mass are not independent.

The goal of this section is to derive a complete set of equations of motion in terms of the osculating values of h, e, θ, and α, where α is the longitude of the periapsis. To do that, we can express the modulus of the derivative of the specific angular momentum in terms of the electrodynamic force:

$$\frac{\mathrm{d}h}{\mathrm{d}t} = -\frac{\Lambda i_{\text{av}}}{\mu_J m} \frac{\mathcal{P}_1(1 + e\cos\theta)^5}{h^{11}} \cos\phi \tag{17}$$

On the other hand, considering the definition of the eccentricity $\boldsymbol{e} = -\boldsymbol{r}/r - (\boldsymbol{h} \times \boldsymbol{v})/\mu_J$, and projecting its derivative with respect to time in the perifocal reference frame, we obtain

$$\frac{\mathrm{d}e}{\mathrm{d}t} = -\frac{\Lambda i_{\text{av}}}{\mu_J m} \frac{(1 + e\cos\theta)^6}{h^{12}} \mathcal{P}_1\mathcal{P}_2 \cos\phi \tag{18}$$

$$\frac{\mathrm{d}\alpha}{\mathrm{d}t} = -\frac{\Lambda i_{\text{av}}}{\mu_J m} \frac{(1 + e\cos\theta)^6}{h^{12}} \mathcal{P}_1\mathcal{P}_3 \cos\phi \sin\theta \tag{19}$$

where the functions $\mathcal{P}_2$ and $\mathcal{P}_3$ have been defined as

$$\mathcal{P}_2(\theta, \phi, e) = \left[2\cos\theta + \frac{e\sin^2\theta}{1 + e\cos\theta} - \tan\phi \sin\theta\right] \tag{20}$$

$$\mathcal{P}_3(\theta, \phi, e) = \left[\frac{2}{e} + \frac{\tan\phi}{e\tan\theta} - \frac{\cos\theta}{1 + e\cos\theta}\right] \tag{21}$$

At last, it is necessary to establish the relation between true anomaly and time. Differentiating the expression of the velocity in cylindrical coordinates, we reach the formula for the variation of the true anomaly with time:

$$\frac{\mathrm{d}\theta}{\mathrm{d}t} = \frac{\mu_J^2(1 + e\cos\theta)^2}{h^3} - \frac{\Lambda i_{\text{av}}(1 + e\cos\theta)^6}{\mu_J m h^{12}} \mathcal{P}_1\mathcal{P}_4 \tag{22}$$

where the function $\mathcal{P}_4$ is defined as follows:

$$\begin{aligned} \mathcal{P}_4(\theta, \phi, e) = \Bigg[&\sin\phi + \cos\phi \tan\theta \left(\frac{2 + e\cos\theta}{1 + e\cos\theta}\right. \\ &\left. - (e + \cos\theta)\left(\frac{2}{e} + \frac{\tan\phi}{e\tan\theta} - \cos\theta\right)\right)\Bigg] \end{aligned} \tag{23}$$

Gathering the results in a system of equations, we have a new system of fourth order:

$$\frac{\mathrm{d}h}{\mathrm{d}t} = -\frac{\Lambda i_{\text{av}}}{\mu_J M_{\text{SC}}} \frac{\mathcal{P}_1(1 + e\cos\theta)^5}{h^{11}} \cos\phi \tag{24}$$

$$\frac{\mathrm{d}e}{\mathrm{d}t} = -\frac{\Lambda i_{\text{av}}}{\mu_J M_{\text{SC}}} \frac{(1 + e\cos\theta)^6}{h^{12}} \mathcal{P}_1\mathcal{P}_2 \cos\phi \tag{25}$$

$$\frac{\mathrm{d}\alpha}{\mathrm{d}t} = -\frac{\Lambda i_{\text{av}}}{\mu_J M_{\text{SC}}} \frac{(1 + e\cos\theta)^6}{h^{12}} \mathcal{P}_1\mathcal{P}_2 \cos\phi \sin\theta \tag{26}$$

$$\frac{\mathrm{d}\theta}{\mathrm{d}t} = \frac{\mu_J^2(1+e\cos\theta)^2}{h^3} - \frac{\Lambda i_{\mathrm{av}}(1+e\cos\theta)^6}{\mu_J m h^{12}}\mathcal{P}_1\mathcal{P}_4 \tag{27}$$

B. Nondimensional Formulation

The use of nondimensional equations instead of the dimensional ones is desirable because it allows us to define the main parameters involved in the capture process. We will use $h_c = h_0$, the initial value of the specific angular momentum, as its characteristic value. Regarding the characteristic time, there are two possible choices: on one hand, the angular velocity of the sideral rotation of Jupiter, Ω, and on the other hand, the time related to the orbital motion, $\tau_c = h_0^3/\mu_J^2$. We will use τ_c as the characteristic time calling the relation between both times γ: $\gamma = \Omega\tau_c$. Using those variables, the nondimensional equations of motion can be expressed as follows:

$$\frac{\mathrm{d}\hat{h}}{\mathrm{d}\tau} = -\hat{\Lambda} i_{\mathrm{av}} \frac{(1+e\cos\theta)^5}{\hat{h}^{11}}\mathcal{P}_1\cos\phi \tag{28}$$

$$\frac{\mathrm{d}e}{\mathrm{d}\tau} = -\hat{\Lambda} i_{\mathrm{av}} \frac{(1+e\cos\theta)^6}{\hat{h}^{12}}\mathcal{P}_1\mathcal{P}_2\cos\phi \tag{29}$$

$$\frac{\mathrm{d}\alpha}{\mathrm{d}\tau} = -\hat{\Lambda} i_{\mathrm{av}} \frac{(1+e\cos\theta)^6}{\hat{h}^{12}}\mathcal{P}_1\mathcal{P}_2\cos\phi\sin\theta \tag{30}$$

$$\frac{\mathrm{d}\theta}{\mathrm{d}\tau} = \frac{(1+e\cos\theta)^2}{\hat{h}^3} - \hat{\Lambda} i_{\mathrm{av}} \frac{(1+e\cos\theta)^6}{\hat{h}^{12}}\mathcal{P}_1\mathcal{P}_4 \tag{31}$$

where $\hat{\Lambda} = (m_t\sigma_c\mu_m^2 R_J^6)/(\rho_v m\tau_c^2 h_0^3)$ is a nondimensional value. The initial conditions needed to integrate the system of Eqs. (28–31) are

$$\hat{h}(0) = 1; \qquad e(0) = e_0; \qquad \alpha(0) = 0 \tag{32}$$

and the initial true anomaly fulfilling the constraint (from $\boldsymbol{E}_m = 0$):

$$\mathcal{P}_1 = 0 \Rightarrow (\cos\phi + e_0\cos(\theta_0+\phi))(1+e_0\cos\theta_0) = \gamma\cos\phi \tag{33}$$

In some situations, it can be useful to express the system as a function of the true anomaly instead of the nondimensional time because that allows us to restrict the integration to the drag arc. Because τ does not appear explicitly in the dynamic equations, the true anomaly will be used as the independent variable, provided that $\mathrm{d}\theta/\mathrm{d}\tau$ is not canceled. This situation is extreme, undesirable, and unlikely to happen. Eventually, the final expression for the dynamic equations is found to be

$$\frac{\mathrm{d}\hat{h}}{\mathrm{d}\theta} = -\hat{\Lambda} i_{\mathrm{av}} \frac{\hat{h}(1+e\cos\theta)^3\mathcal{P}_1\cos\phi}{\hat{h}^9 - \hat{\Lambda} i_{\mathrm{av}}(1+e\cos\theta)^4\mathcal{P}_1\mathcal{P}_4} \tag{34}$$

$$\frac{\mathrm{d}e}{\mathrm{d}\theta} = -\hat{\Lambda} i_{\mathrm{av}} \frac{(1+e\cos\theta)^4\mathcal{P}_1\mathcal{P}_2\cos\phi}{\hat{h}^9 - \hat{\Lambda} i_{\mathrm{av}}(1+e\cos\theta)^4\mathcal{P}_1\mathcal{P}_4} \tag{35}$$

$$\frac{\mathrm{d}\alpha}{\mathrm{d}\theta} = -\hat{\Lambda} i_{\mathrm{av}} \frac{(1+e\cos\theta)^4\mathcal{P}_1\mathcal{P}_3\cos\phi\sin\theta}{\hat{h}^9 - \hat{\Lambda} i_{\mathrm{av}}(1+e\cos\theta)^4\mathcal{P}_1\mathcal{P}_4} \tag{36}$$

with the initial conditions:

$$\hat{h}(\theta_0) = 1; \qquad e(\theta_0) = e_0; \qquad \alpha(\theta_0) = 0 \tag{37}$$

IV. Attitude Dynamics

From the expressions obtained in the previous section, it can be noted that the attitude plays an important role in the motion of the center of mass. It is therefore compulsory to study the attitude behavior of the tethered systems. This paragraph is intended to present the attitude dynamics in a comprehensive way.

The equation that governs the attitude dynamics is the equation of the angular momentum:

$$\frac{\mathrm{d}\boldsymbol{L}_G}{\mathrm{d}t} = \boldsymbol{M} \tag{38}$$

where the angular momentum can be expressed as a function of the angular velocity and the inertia tensor: $\boldsymbol{L}_G = \bar{\bar{I}}_G{}^{\circ}\boldsymbol{\omega}$. In turn, the angular velocity is related to the unitary vector u in the tether direction, assuming that the tether is a rigid body and remains straight: $\boldsymbol{\omega} = \boldsymbol{u}\times\dot{\boldsymbol{u}} + (\boldsymbol{\omega}\cdot\boldsymbol{u})\boldsymbol{u}$. Therefore, Eq. (38) can then be rewritten as

$$\boldsymbol{u}\times\ddot{\boldsymbol{u}} = \frac{1}{I_s}\boldsymbol{M} \tag{39}$$

The torques considered in this work will be the gravity gradient and the electrodynamic torque. The momentum due to the gravity forces is analyzed in first place. It can be established as

$$M_{gg} = -\int_{\Omega_0}(\boldsymbol{r}-\boldsymbol{r}_G)\times\frac{\mu_J}{r^3}\boldsymbol{r}\,\mathrm{d}m = \boldsymbol{r}_G\times\int_{\Omega_0}\frac{\mu_J}{r^3}\boldsymbol{r}\,\mathrm{d}m \tag{40}$$

where $\boldsymbol{r}$ and $\boldsymbol{r}_G$ are the position vector of each mass element and the center of mass of the tethered system, respectively, and Ω_0 is the volume of the whole system. Considering $\boldsymbol{r} = \boldsymbol{r}_G + \boldsymbol{s}$ with $|\boldsymbol{s}| \ll |\boldsymbol{r}_G|$, the first approximation of the gravity gradient is as follows:

$$\boldsymbol{M}_{gg} = \boldsymbol{r}_G\times\int_{\Omega_0}\frac{\mu_J}{|\boldsymbol{r}_G+\boldsymbol{s}|^3}\boldsymbol{s}\,\mathrm{d}m \asymp \frac{3\mu_J}{r_G^5}\boldsymbol{r}_G\times(\bar{\bar{I}}_G{}^{\circ}\boldsymbol{r}_G) \tag{41}$$

Expressing the vector $\boldsymbol{u}$ in the inertial reference frame, $\boldsymbol{u} = \cos\psi\boldsymbol{i} + \sin\psi\boldsymbol{j}$, the vector product $\boldsymbol{u}\times\ddot{\boldsymbol{u}}$ is a function of the angle ψ:

$$\boldsymbol{u}\times\ddot{\boldsymbol{u}} = \ddot{\psi}\ \boldsymbol{k} = \frac{1}{I_s}\boldsymbol{M} \tag{42}$$

On the other hand, naming $\boldsymbol{r}_G = r_G\boldsymbol{u}_r$, the identity $\boldsymbol{u}_r = (\boldsymbol{u}_r\cdot\boldsymbol{u})\boldsymbol{u} + \boldsymbol{u}\times(\boldsymbol{u}_r\times\boldsymbol{u})$ yields

$$\bar{\bar{I}}_G\circ\boldsymbol{u}_r = I_s\boldsymbol{u}\times(\boldsymbol{u}_r\times\boldsymbol{u}) = I_s\{\boldsymbol{u}_r - \boldsymbol{u}(\boldsymbol{u}_r\cdot\boldsymbol{u})\} \tag{43}$$

The gravity torque can be therefore expressed as

$$\boldsymbol{M}_{gg} = \frac{3\mu_J}{r_G^3}I_s(\boldsymbol{u}\times\boldsymbol{u}_r)(\boldsymbol{u}_r\cdot\boldsymbol{u}) \tag{44}$$

Taking into account that $\boldsymbol{u}_r = \cos(\alpha+\theta)i + \sin(\alpha+\theta)\boldsymbol{j}$, the final expression for the equation of the angular momentum is stated as

$$\ddot{\psi} = \frac{3\mu_J}{r_G^3}\sin(\theta+\alpha-\psi)\cos(\theta+\alpha-\psi) \tag{45}$$

On the other hand, the electrodynamic torque due to the Lorentz force acting over the tether can be computed as

$$\boldsymbol{M}_{\mathrm{ed}} = \int_{\Omega}(s\boldsymbol{u}\times\boldsymbol{F}_{\mathrm{ed}}^{ds})\,\mathrm{d}s \tag{46}$$

Considering the previous definition of the electrodynamic force [Eq. (14)] and assuming the same hypothesis used to simplified its expression in the previous analysis, we obtain

$$\boldsymbol{M}_{\text{ed}} = \boldsymbol{u} \times (\boldsymbol{u} \times \boldsymbol{B}) \int_{\Omega} sI \, \mathrm{d}s \tag{47}$$

With respect to the derivation of the force, there is a slight difference regarding the current, because the value of the integral is no longer the average value but the first momentum of the current profile.

Dimensional:

$$L_t^2 I_{m1} = \int_{\Omega} sI \, \mathrm{d}s \tag{48a}$$

Nondimensional:

$$I_{m1} = \sigma_c E_m d_t h_t i_{m1}(\ell_t) \tag{48b}$$

That yields the following relation:

$$\boldsymbol{M}_{\text{ed}} = -B(r)^2 \frac{\sigma_c m_t L_t}{\rho_v} i_{m1} (v_\theta^{\text{rel}} \cos\phi - v_r^{\text{rel}} \sin\phi) \boldsymbol{u}_z \tag{49}$$

The value of the moment of inertia as a function of the parameters of the geometry of mass is gathered in Eq. (6). Introducing this expression and the term of the electrodynamic torque in the attitude equation, we can obtain the relation for the evolution of the angular velocity.

Besides, as it was made for the motion of the center of mass, the equation of the attitude dynamics can be expressed in nondimensional form. Using the same characteristic magnitudes, the results are gathered in the following lines. Describing the attitude by means of the inertial angle ψ:

$$\frac{d^2\psi}{d\tau^2} = -\frac{3}{2}\frac{(1+e\cos\theta)^3}{\hat{h}^6}\sin(2(\psi-\theta-\alpha)) - \frac{\kappa i_{m1}}{(3\sin^2(2\chi)-2\Gamma)}\frac{(1+e\cos\theta)^6}{\hat{h}^{13}}\mathcal{P}_1 \tag{50}$$

or in terms of the angle ϕ:

$$\frac{d^2\phi}{d\tau^2} = -\frac{d^2\theta}{d\tau^2} - \frac{d^2\alpha}{d\tau^2} - \frac{3}{2}\frac{(1+e\cos\theta)^3}{\hat{h}^6}\sin(2\phi) - \frac{\kappa i_{m1}}{(3\sin^2(2\chi)-2\Gamma)}\frac{(1+e\cos\theta)^6}{\hat{h}^{13}}\mathcal{P}_1 \tag{51}$$

where

$$\kappa = \frac{12\mu_m^2 R_J^6 \sigma_c \mu_J^3}{L_t h_0^7 \rho_v} \tag{52}$$

V. Control on Nonrotating Tethers

Because of the strong coupling between attitude and center of mass motions, control of the former constitutes a matter of the first relevance. That is due to the fact that having the right orientation is compulsory to complete the capture maneuver successfully. In this section, the feasibility of obtaining the desired attitude without using external means (other than the gravitational and electrodynamic forces) is explored.

A. Assessment of Control Authority

The first question addressed is whether or not the electrodynamic torque is able to keep the attitude of the tether controlled. Therefore, the required control torque and the operational limits of the electrodynamic torque will be analyzed to eventually compare the both of them.

1. *Needed Torque*

The attitude dynamics are governed by Eq. (51) in terms of the angle ϕ. To evaluate the torque needed to maintain a prefigured attitude profile, we will consider the following function:

$$\mathcal{G}(\tau) = -\left(\frac{d^2\phi}{d\tau^2} + \frac{d^2\theta}{d\tau^2} + \frac{d^2\alpha}{d\tau^2} + \frac{3}{2}\frac{(1+e\cos\theta)^3}{\hat{h}^6}\sin(2\phi)\right) \times \frac{\kappa \hat{h}^{13}(\tau)}{(1+e(\tau)\cos\theta(\tau))^6 \mathcal{P}_1(\hat{h}(\tau), e(\tau), \theta(\tau))} \tag{53}$$

According to Eq. (51), the needed torque can be written as

$$i_{m1}^{\text{need}} = (3\sin^2(2\chi) - 2\Gamma)\mathcal{G}(\tau) \tag{54}$$

The function $\mathcal{G}(\tau)$ can be obtained as a result of the integration of the equations of motion for a given attitude profile $\phi(\tau)$. It should be noted that this expression is only valid for $\mathcal{P}_1 \geq 0$ (i.e., only along the arc where it is possible to generate drag). On the other hand, χ and Γ are functions of the geometry of mass of the system. And consequently, the function $\mathcal{F}_{I_s} = (3\sin^2(2\chi) - 2\Gamma)$ is computed given the values of the end masses m_1 and m_2 and the tether mass m_t. The values corresponding the self-balance configurations (with $\chi \in \sim[40, 50 \text{ deg}]$) vary between 1 and 3. Accordingly, the influence of this factor is not expected to be determinant in the controllability.

On the other hand, the function $\mathcal{G}(\tau)$ must be computed as a result of the integration of the equations of motion. A reference case is chosen to perform the aforementioned integration, characterized by the parameters gathered in Table 1. Additionally, an attitude profile should be established. We will consider three cases regarding the suitability from the point of view of the electrodynamic forces that can be generated: 1) $\phi = 0$ (the tether is pointing continuously toward Jupiter), 2) $\psi = 0$ (the tether keeps a fix inertial orientation), and 3) $\boldsymbol{u} \cdot \boldsymbol{v}^{\text{rel}} = 0$ (the tether is forced to be perpendicular to both the relative velocity to the plasma and the magnetic field). The results obtained are shown in the last paragraph of this section.

2. *Electrodynamic Torque*

In Eq. (54), the left term depends on the current profile along the tether. In fact, i_{m1} is the nondimensional first order moment of the current respect to the center of mass, i.e.,

$$i_{m1} = \int_0^{\ell_t} (\xi_G - \xi) i(\xi) \, \mathrm{d}\xi = \ell_t \cos^2(\chi) U_1(\ell_t, \Omega_t) - U_2(\ell_t, \Omega_t) \tag{55}$$

where $U_1(\ell_t, \Omega_t) = \int_0^{\ell_t} i(\xi) \, \mathrm{d}\xi$, and $U_2(\ell_t, \Omega_t) = \int_0^{\ell_t} \xi i(\xi) \, \mathrm{d}\xi$. To compute the values of U_1 and U_2, it is necessary to solve the two-boundary-value problem for the current $i(\xi)$ as it is exposed in Peláez and Sanjurjo-Rivo [21]. With that formulation, U_1 and U_2 are

$$U_1(\ell_t, \Omega_t) = \ell_t + \varphi_C - \varphi_A \tag{56}$$

Table 1 Maneuver and tether characteristics for the analysis of the required torque

Manuever and tether parameters	Values
Periapsis radius (initial hyperbolic trajectory)	1.42 R_J
Initial velocity	5.64 km/s
Tether length	100 km
Tether thickness	0.05 mm
Tether width	30 mm
Tether mass	405 kg
Spacecraft mass	905 kg
Mass angle χ	40 deg
Tether material	Aluminum

$$U_2(\ell_t, \Omega_t) = \varphi_C \ell_t + \frac{\ell_t^2}{2} - \frac{4}{3}(1 - i_B)^{5/3}\left[\int_0^{v_0} \sinh^{5/3}(\zeta)\,\mathrm{d}\zeta - \frac{1}{\mu^{4/3}}\int_0^{v_T} \sinh^{5/3}(\zeta)\,\mathrm{d}\zeta\right] \tag{57}$$

We are interested on the operational limits of the control, $\Omega_t = 0$ and $\Omega_t \to \infty$. In the first case, $\Omega_t = 0$, we have $\varphi_C = 0$, $\ell_t = \xi_B$, and therefore

$$U_1(\ell_t, 0) = \ell_t - \varphi_A \tag{58}$$

$$U_2(\ell_t, 0) = \frac{\ell_t^2}{2} - \frac{4}{3}(1 - i_B)^{5/3}\int_0^{v_0} \sinh^{5/3}(\zeta)\,\mathrm{d}\zeta \tag{59}$$

In the second case, we have $i_C = 0$ and $v_T = v_0$, and then

$$U_1(\ell_t, \to \infty) = \ell_t + \varphi_C - \varphi_A \tag{60}$$

$$U_2(\ell_t, \to \infty) = \frac{\ell_t^2}{2} + \varphi_C \ell_t - \frac{4}{3}(1 - i_B)^{5/3} \times \int_0^{v_0} \sinh^{5/3}(\zeta)\,\mathrm{d}\zeta\left(1 - \frac{1}{\mu^{4/3}}\right) \tag{61}$$

In the next paragraph, the limits $i_{m1}(\Omega_t = 0)$ and $i_{m1}(\Omega_t \to \infty)$ are plotted in the same graphs as the needed values i_{m1}^{need} as functions of ℓ_t and τ.

3. Comparison

In Fig. 2, we compare the needed values of the electrodynamic torque and its limits of operation for the first of the attitude profiles proposed (i.e., the tether pointing continuously toward Jupiter). The needed values are represented by black squares while the limits of operation appear as black lines.

The results obtained for the other two attitude profiles are similar to those shown in Fig. 2. The electrodynamic torque, which acts as control power, is small to counteract the gravitational torque. Furthermore, the electrodynamic torque is only available during the drag arc, and therefore there is no compensating torque outside the drag sphere. Therefore, a complete control of the tether attitude following an arbitrary predefined trajectory is not possible. Nevertheless, the tethered system would be able to complete the capture maneuver with negligible angular velocity with the feedback control, which is described next.

B. Feedback Control

1. Nominal Attitude Profile

From the results exposed in Scheeres et al. [22] and Scheeres [23], the change in angular momentum during an equatorial flyby will only have a component along the z axis proportional to $\sin 2(\omega + \Omega)$. We can cancel this term by means of making the x axis of the tether fixed reference frame at the periapsis points toward the center of mass of the planet, where the x axis in the body fixed reference frame is defined to lie along the axis of minimum momentum of inertia. That is, the tether should be aligned with the local vertical in the periapsis passage.

As a first step, we will analyze the motion of the tethered system when the electrodynamic forces are not present. Our objective will be to obtain a solution that fulfills the condition of keeping the tether without spin at the end of the flyby. The nondimensional form of the equation that governs the attitude in terms of an inertial angle ψ is Eq. (50). To get the necessary initial condition in the angle ψ to keep the tether nonrotating, Eq. (50) should be solved with the following boundary conditions:

$$\dot{\psi}(\theta_0) = 0 \tag{62}$$

$$\psi(\theta = 0) = 0 \tag{63}$$

One relevant issue in this approach is where the initial condition is considered to be. Because the angle that defines the asymptote of the hyperbola is $\theta_a = \arccos(-1/e)$, where e is its eccentricity, the initial angle θ_0 must be a fraction of θ_a. The solution can vary slightly when different values of θ_0 are considered. When we take $\theta_0 = 0.99\theta_a$, the initial angle ψ_0, which provides no change of the angular momentum, is $\psi_0 \approx -57.2$ deg. In Fig. 3, the central line represents the solution along the whole trajectory in terms of the inertial angle and the nondimensional angular velocity.

The result shows the profile of the inertial angle is antisymmetric respect to $\theta = 0$. Furthermore, the value of ψ is close to 0 in the neighborhood of the periapsis (being exactly zero in the periapsis), which represents a convenient profile in terms of the generation of electrodynamic force. In turn, the desired final value of the angular velocity has been obtained. Nevertheless, it experiences a large excursion reaching its minimum at the periapsis and being its profile symmetric respect to $\theta = 0$.

Other aspects that should be assessed include the sensitivity of the solution that has been obtained. In Fig. 3, the evolution of the inertial angle and the nondimensional angular velocity is presented when the initial condition in ψ is modified by 1% and compared to the nominal solution. The nominal solution (zero final angular velocity) is obtained with $\psi_0^{\text{nominal}} = -57.2$ deg, while the other two lines are obtained with $\psi_0 = 1.01\psi_0^{\text{nominal}}$ and $\psi_0 = 0.99\psi_0^{\text{nominal}}$. From the results of Fig. 3, we can conclude that slight initial deviations from the nominal value in the initial angle yields an important difference in the final nondimensional angular velocity.

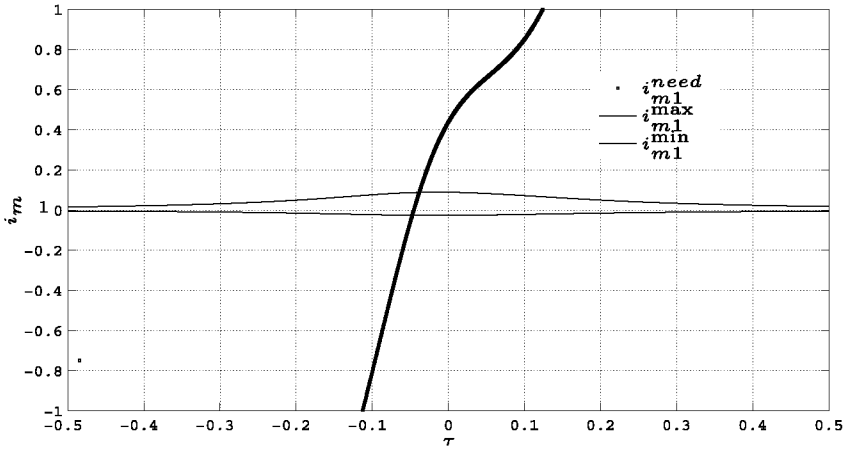

Fig. 2 Needed values of i_{m1} as a function of ℓ_t during the capture (black squares) and the control limits of i_{m1} (black lines); control law: $\phi \equiv 0$.

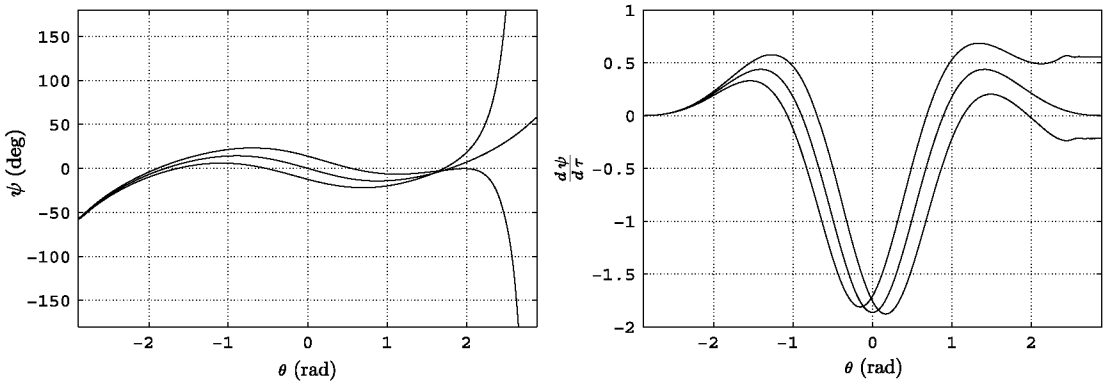

Fig. 3 Comparison of the different evolution of the angular variables regarding the initial condition in ψ.

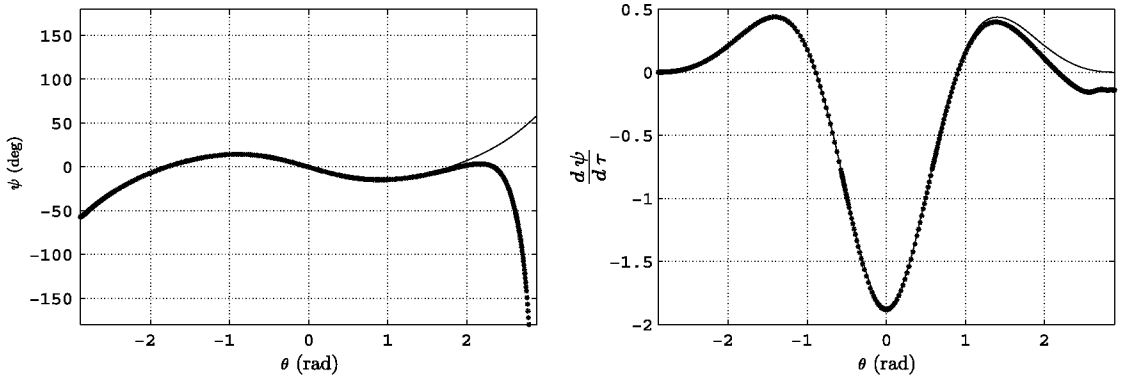

Fig. 4 Comparison of the different evolution of the angular variables regarding whether the electrodynamic forces are present (dots) or not (line).

Hereafter, the situation when electrodynamic forces are considered is analyzed. A comparison between the nominal solution and the capture trajectory is presented in Fig. 4. The initial angle ψ_0 is the same in both cases. The control variable Ω_t has been set to zero during the whole drag arc.

As it can be noted in Fig. 4, the effect of the electrodynamic torque during the drag arc has an effect of the same order as the small perturbations in the initial value of the inertial angle ψ. The electrodynamic torque can be controlled using the free parameter Ω_t as a control variable. In particular, we can cancel out the value of the electrodynamic torque adjusting the value of Ω_t to Ω_{SBET}, the value of the nondimensional load for a SBET [6,7,13]. In fact, because the electrodynamic perturbation torque no longer affects the attitude dynamics, this control strategy will lead to an inertial angle profile identical to that showed in Fig. 3 when the appropriate initial condition is chosen. Additionally, small variations of Ω_t around Ω_{SBET} can be performed to correct the attitude when the actual inertial angle differs from the nominal one. In the next paragraph, a feedback control is proposed to deal with these small corrections.

2. *Feedback Control Definition*

In this paragraph, we pose the problem of the control around the previously defined nominal trajectory. The nominal orbit is determined by the evolution of the state vector: $\boldsymbol{y}^N(\tau)$ where: $\boldsymbol{y} = \{\hat{h}, e, \alpha, \theta, \psi, \dot{\psi}\}^T$. On the other hand, the control variable $\Omega_t^N(\tau) = \Omega_{\text{SBET}}$ for the whole nominal path.

The dynamics of the system can be described as a system of differential equations with the following dependence:

$$\frac{\mathrm{d}\boldsymbol{y}}{\mathrm{d}\tau} = \mathcal{F}(\boldsymbol{y}) + i_{\text{av}}(\Omega_t)\mathcal{G}(\boldsymbol{y}) \tag{64}$$

The linearization around the nominal trajectory leads to

$$\frac{\mathrm{d}(\delta\boldsymbol{y})}{\mathrm{d}\tau} = \left(\left.\frac{\partial\mathcal{F}}{\partial\boldsymbol{y}}\right|_{y^N} + i_{\text{av}}(\Omega_t^N)\cdot\left.\frac{\partial\mathcal{G}}{\partial\boldsymbol{y}}\right|_{y^N}\right)\delta\boldsymbol{y} + \mathcal{G}(\boldsymbol{y}^N)\left.\frac{\partial i_{\text{av}}}{\partial\Omega_t}\right|_{\Omega_t^N}\delta\Omega_t \tag{65}$$

where $\delta\boldsymbol{y}$ is the variation of the state vector, and $\delta\Omega_t$ is the variation of the control variable. In a more compact form, we will have

$$\frac{\mathrm{d}(\delta\boldsymbol{y})}{\mathrm{d}\tau} = \mathcal{A}(\boldsymbol{y}^N, \Omega_t^N)\delta\boldsymbol{y} + \mathcal{Z}(\boldsymbol{y}^N, \Omega_t^N)\delta\Omega_t \tag{66}$$

The objective of the control is to chose $\delta\Omega_t$ in such a way that the system will not be unstable. A first approximation consistd of using proportional control: $\delta\Omega_t = \boldsymbol{c}^T\delta\boldsymbol{y}$. That approach yields

$$\frac{\mathrm{d}(\delta\boldsymbol{y})}{\mathrm{d}\tau} = [\mathcal{A}(\boldsymbol{y}^N, \Omega_t^N) + \mathcal{Z}(\boldsymbol{y}^N, \Omega_t^N)c^T]\delta\boldsymbol{y} \tag{67}$$

The problem then can be formulated as the determination of $\boldsymbol{c}$, in general a function of time, in such a way that the system becomes stable.

3. *One-Dimensional Feedback Control*

Nevertheless, given that the instability is related to the attitude of the tether, the simpler study of the linearized attitude dynamics is considered. It is expected that small variations of the control variable have a small impact on the motion of the center of mass. Thus, when the rest of the state variables are ignored, the linearized system can be written as

$$(\delta\ddot{\psi}) = \mathcal{A}'(\boldsymbol{y}^N, \Omega_t^N)\delta\psi + \mathcal{B}'(\boldsymbol{y}^N, \Omega_t^N)\delta\Omega_t \tag{68}$$

It turns out to be a second-order differential equation on $\delta\psi$. In this one-dimensional analysis, the proportional control law can be

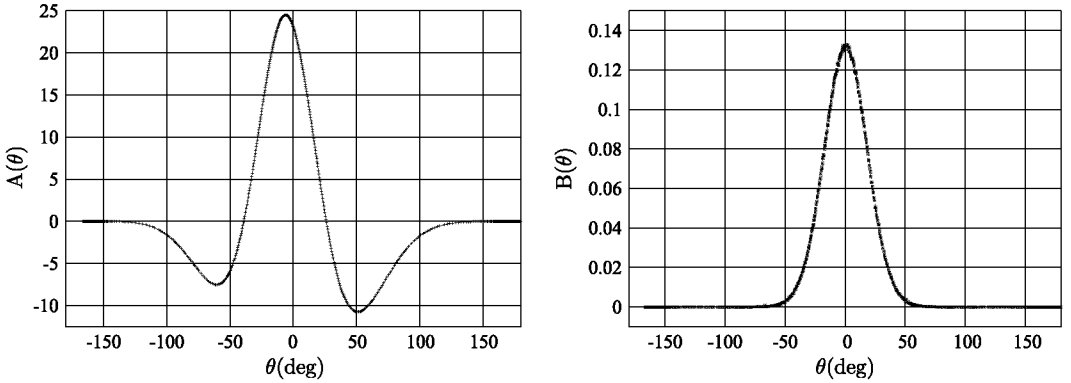

Fig. 5 Variation of $\mathcal{A}'(\theta)$ and $\mathcal{B}'(\theta)$ as a function of the true anomaly θ.

expressed as $\delta\Omega_t = \mathcal{K}' \cdot \delta\psi$. When the control law is considered in the previous equation, the resultant relation between the angular deviation from the nominal profile $\delta\psi$ and its second derivative is

$$(\ddot{\delta\psi}) = (\mathcal{A}' + \mathcal{B}'\mathcal{K}')\delta\psi \tag{69}$$

Therefore, the condition that $\mathcal{K}'$ must fulfill to provide stability to the attitude motion is stated as $\mathcal{A}' + \mathcal{B}'\mathcal{K}' < 0 \,\forall\, \tau$. The values of $\mathcal{A}'$ and $\mathcal{B}'$ depend on the nominal trajectory, and they have the following form:

$$\mathcal{A}'(\tau) = \frac{\mathcal{K} i_{m1}(1 + e_0\cos(\theta_0))^6}{\hat{h}_0^{13}}\left[-\sin(\psi_0 - \theta_0 - \alpha_0) - e_0\sin(\psi_0 - \alpha_0) + \frac{\gamma h_0^3 \sin(\psi_0 - \theta_0 - \alpha_0)}{1 + e_0\cos(\theta_0)}\right] + \frac{3(1 + e_0\cos\theta_0)^3}{\hat{h}^3}\cos(2(\psi_0 - \theta_0 - \alpha_0)) \tag{70}$$

$$\mathcal{B}'(\tau) = \mathcal{K}\frac{\partial i_{m1}}{\partial\Omega_t}\frac{(1 + e_0\cos\theta_0)^6}{\hat{h}_0^{13}}\left[\cos(\psi_0 - \theta_0 - \alpha_0) + e_0\cos(\psi_0 - \alpha_0) - \frac{\gamma h_0^3\cos(\psi_0 - \theta_0 - \alpha_0)}{1 + e_0\cos(\theta_0)}\right] \tag{71}$$

In Fig. 5, the functions $\mathcal{A}'$ and $\mathcal{B}'$ are plotted as a function of the true anomaly θ. We can note that the aspect of $\mathcal{A}'$ is convenient because it does not present positive values outside the part of the orbit where the electrodynamic torque is different from zero. Thus, the motion outside those limits is not unstable. However, the values of $\mathcal{B}'$ are significantly smaller than those of $\mathcal{A}'$, and therefore high gains should be used. Moreover, if we chose $\mathcal{K}'$ in the following way:

$$\mathcal{K}' = \begin{cases} 0 & \mathcal{B}' = 0 \\ -\frac{\mathcal{A}' + |\mathcal{A}'|}{2\mathcal{B}'} & \mathcal{B}' \neq 0 \end{cases} \tag{72}$$

then the stability condition is fulfilled (while $\mathcal{A}' < 0$ when $\mathcal{B}' = 0$).

Nevertheless, there exists a limit in this kind of control due to the fact Ω_t cannot be negative: $\Omega_t^N + \delta\Omega_t \geq 0$. The nominal value of the nondimensional electric load is the self-balanced one, and then we rewrite the last expression as $\delta\Omega_t \geq -\Omega_{\text{SBET}}$. This condition represents a limit on the control authority for this control law. In terms of the maximum controllable angle, we obtain

$$\delta\Omega_t \geq -\Omega_{\text{SBET}} \Rightarrow -\frac{\Omega_{\text{SBET}}}{|\mathcal{K}'|} \leq \delta\psi \leq \frac{\Omega_{\text{SBET}}}{|\mathcal{K}'|} \tag{73}$$

The limits are represented in Fig. 6 as a function of the true anomaly. Within this limit, the attitude dynamics are governed by

$$(\ddot{\delta\psi}) = \frac{\mathcal{A}' + |\mathcal{A}'|}{2}\delta\psi \qquad \mathcal{B}' = 0 \tag{74}$$

$$(\ddot{\delta\psi}) = \mathcal{A}'\delta\psi \qquad \mathcal{B}' \neq 0 \tag{75}$$

The linearized equations of motion for the attitude dynamics are integrated for different initial conditions (i.e., for different initial deviations from the nominal path). The results are shown in Fig. 7. It can be noted that deviations in angular momentum are of more concern than the deviation on initial angle. In fact, all initial angles that allow a linearized treatment are controlled, providing that the excursions on initial angular velocity are well constrained.

VI. Thermal Analysis

In Gallagher et al. [10], overheating of the tether turned out to be one of the limiting factors for Jupiter capture. To estimate the effect of the heating problem, a thermal analysis is carried out hereafter. The energy equation determining the temperature $T(s)$ of an element of tether length δs is

$$d_t h_t \delta s \times \rho_t c_t \frac{\partial T}{\partial t} = \dot{Q}_{\text{th}}\delta s + \dot{Q}_4\delta s + \dot{Q}\delta s + \dot{Q}_A\delta s - 2d_t\delta s \times \epsilon_t\sigma_B T^4 + d_t h_t \delta s \times K_t\frac{\partial^2 T}{\partial s^2} \tag{76}$$

where d_t and h_t are the width and thickness of the tether tape, respectively; ρ_t, c_t, ϵ_t, and K_t are the tether density, specific heat, emissivity, and thermal conductivity, respectively; σ_B is the Stefan–Boltzmann constant $\sigma_B = 5.68 \cdot 10^{-8}$ W/m$^2 \cdot$ K^4); and the contributions to the thermal energy are the following.

1) Internal heating power $\dot{Q}_{\text{th}}\delta s$ is made of two contributions [2], one due to the ohmic dissipation and other due to the impact of collected electrons:

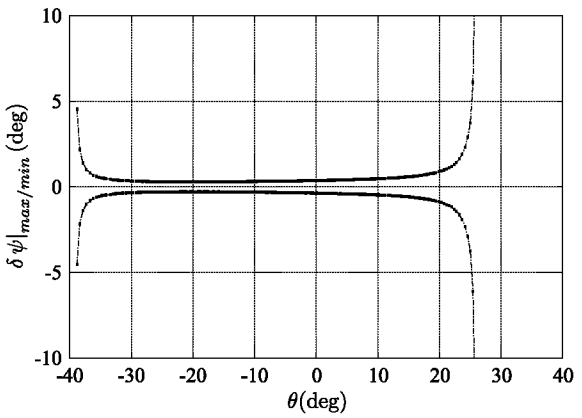

Fig. 6 Maximum value of $\delta\psi$ that can be controlled with this control approach.

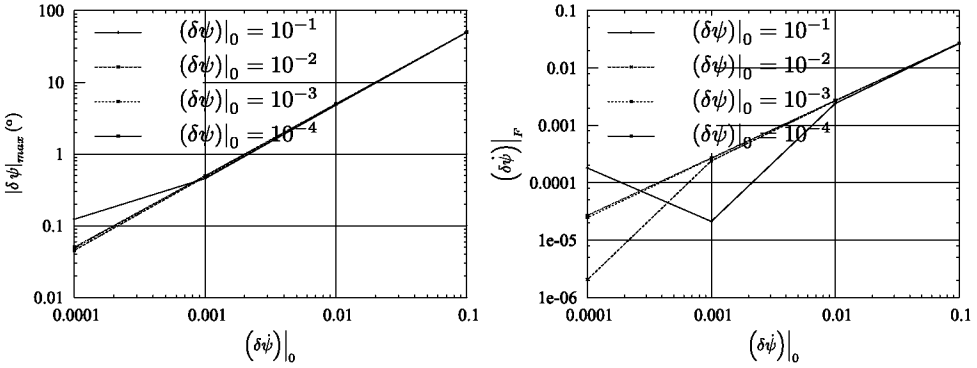

Fig. 7 Maximum absolute value of $\delta\psi$ and final value of the deviation in angular velocity $\dot{\delta\psi}$ as a function of the initial deviations from the nominal path.

$$\dot{Q}_{\text{th}}\delta s = \frac{I(s)^2}{\sigma_c d_t h_t}\delta s + \Phi\frac{\mathrm{d}I(s)}{\mathrm{d}s}\delta s \tag{77}$$

where σ_c is the resistivity of the tether, $I(s)$ is the current, and Φ is the bias between plasma and tether. Note that the resistivity of the tethers and the current depend on the temperature. Nevertheless, as a first approximation, resistivity is to be considered constant. Using the nondimensional variables defined in the study of the current along the tether $I(s) = \boldsymbol{E}_m\sigma_c d_t h_t i$, $\Phi = \varphi\boldsymbol{E}_m L_\star$ and $s = \xi L_\star$, the result is

$$\dot{Q}_{\text{th}}\delta s = E_m^2\sigma_c d_t h_t\left[i^2 + \varphi\frac{\mathrm{d}i}{\mathrm{d}\xi}\right]\delta s \tag{78}$$

2) Jupiter infrared radiation $\dot{Q}_4$; the form of this contribution is [24]

$$\dot{Q}_4\delta s = 2d_t\delta s \times F^o\sigma_B T_J^4\epsilon_t \tag{79}$$

where $\boldsymbol{F}^o$ is the view factor of the tether for Jupiter, and T_J is the black-body temperature of Jupiter.

3) Sun radiation $\dot{Q}$; the expression for the sun radiation can be written as [24]

$$\dot{Q}\delta s = d_t\delta s \times \sigma_a\Psi\Phi \tag{80}$$

where σ_a is the tether absorption coefficient, Ψ is the shining factor, and Φ is the solar flux.

4) Jupiter albedo radiation $\dot{Q}_A$; its intensity is given by [24]

$$\dot{Q}_A\delta s = 2d_t h_t\delta s \times F^o\tau_A\Phi\sigma_a\cos\varsigma \tag{81}$$

where τ_A denotes the Jupiter albedo, and ς represents the sun zenith angle (i.e., the reflection angle of sun rays on Jupiter).

To evaluate the importance of each contribution, we will substitute Eqs. (78–81) in Eq. (76), using the nondimensional variables $\eta = s/L_t$ and $\tau = t/\tau_c$, where $\tau_c = h_0^3/\mu_J^2$. The latter is the characteristic time of the hyperbolic initial trajectory. This yields

$$\begin{aligned}\frac{\partial T(\eta,\tau)}{\partial\tau} &= \frac{E_m^2\sigma_c\tau_c}{\rho_t c_t}\left[i^2(\xi) + \varphi(\xi)\frac{\mathrm{d}i(\xi)}{\mathrm{d}\xi}\right]\\ &- \frac{\epsilon_t\sigma_{\boldsymbol{B}}\tau_c}{h_t\rho_t c_t}[T^4(\eta,\tau) - 2F^oT_J^4] +\\ &+ \frac{\Phi\sigma_a\tau_c}{h_t\rho_t c_t}[\Psi + 2F^o\tau_A\cos\varsigma] + \frac{K_t\tau_c}{L_t^2\rho_t c_t}\frac{\partial^2 T(\eta,\tau)}{\partial\eta^2}\end{aligned} \tag{82}$$

The relation between both nondimensional lengths is $\xi = \ell_t\eta$. Using the values of aluminum, density $\rho_t = 2700$ kg/m^3, specific heat $c_t \approx 900$ J/kg · K, thermal conductivity $K_t \approx 2.37$ J/m · s · K, and resistance $\sigma_c = 3.7668 \cdot 10^7$ $1/(\Omega \cdot \text{m})$, and considering that τ_c is in the interval $\tau_c \in [5.4 \cdot 10^3, 14 \cdot 10^3]$ s, the order of magnitude of the conductivity term in Eq. (82) is

$$\frac{K_t\tau_c}{L_t^2\rho_t c_t}\frac{\partial^2 T(\eta,\tau)}{\partial\eta^2} \sim \frac{K_t\tau_c}{L_t^2\rho_t c_t} \sim 10^{-12} \tag{83}$$

Hence, we do not take this term into account hereafter. We are interested, in the first place, in knowing the steady temperature before the capture maneuver. In that situation, the left term of the equation vanishes (by assumption the temperature does not vary), and there is no internal heating because the electrodynamic tether is switched off. Therefore, the stationary temperature T_0 is

$$T_0^4 = 2F^oT_J^4 + \frac{\sigma_a\Phi}{\epsilon_t\sigma_{\boldsymbol{B}}}[\Psi + 2F^o\tau_A\cos\varsigma] \tag{84}$$

Jupiter's black-body temperature is about $T_J \asymp 110$ K[§], and the solar flux at Jupiter is about $\Phi \asymp 50.5$ W/m^2[§]. The values of other parameters that are involved are more difficult to specify. We will take approximations for all of them. The view factor F^o can vary between 0 and 1; we will take $F^o \approx 0.5$ because it is a conservative limit for vertical tethers [24]. Besides, we neglect variations on the Jupiter albedo, and we will consider an average value $\tau_A \approx 0.34$[§]. The emissivity and the absorption coefficients of the aluminum are in the ranges: $\epsilon_t \in [0.02, 0.45]$ and $\sigma_a \in [0.1, 0.9]$ [24]. We then choose values $\epsilon_t \approx 0.4$, $\sigma_a \approx 0.5$. Finally, we will consider the shining factor $\Psi \approx 0.5$ and the sun zenith angle such that $\cos\varsigma \approx 0.5$. In these conditions, the value of the stationary temperature before the capture maneuver is $T_0 \approx 172$ K. Further, we can neglect the variations of all these parameters during capture so that we can rewrite Eq. (82) as follows:

$$\frac{\partial\mathcal{T}(\eta,\tau)}{\partial\tau} = \frac{E_m^2\sigma_c\tau_c}{\rho_t c_t T_0}\left[i^2(\xi) + \varphi(\xi)\frac{\mathrm{d}i(\xi)}{\mathrm{d}\xi}\right] - \frac{\epsilon_t\sigma_B\tau_c T_0^3}{h_t\rho_t c_t}[\mathcal{T}^4(\eta,\tau) - 1] \tag{85}$$

where $\mathcal{T}(\eta,\tau) = T(\eta,\tau)/T_0$. Because the conductivity along the tether is negligible, we are assuming that $\mathcal{T}(\eta,\tau) \equiv \mathcal{T}(\tau)$. Then, we can integrate the equation along the tether. Considering that

$$\begin{aligned}\int_0^{\ell_t}\left(i^2(\xi) + \varphi(\xi)\frac{\mathrm{d}i}{\mathrm{d}\xi}\right)\mathrm{d}\xi &= \int_0^{\ell_t} i^2\,\mathrm{d}\xi + \varphi i\big|_0^{\ell_t} - \int_0^{\ell_t}(i^2 - 1)\,\mathrm{d}\xi\\ &= \varphi_C i_C + U_1\end{aligned} \tag{86}$$

the final form of the energy equation will be

$$\frac{\mathrm{d}\mathcal{T}(\tau)}{\mathrm{d}\tau} = \frac{E_m^2\sigma_c\tau_c}{\rho_t c_t T_0}\frac{(\varphi_C i_C + U_1)}{\ell_t} - \frac{\epsilon_i\sigma_B\tau_c T_0^3}{h_t\rho_t c_t}[\mathcal{T}^4 - 1] \tag{87}$$

Because of the definition of the nondimensional temperature $\mathcal{T}$, the initial condition at the beginning of the capture maneuver $\mathcal{T}(0) = 1$.

[§]Data available online at http://nssdc.gsfc.nasa.gov/planetary/factsheet/jupiterfact.html [retrieved Nov. 2012].

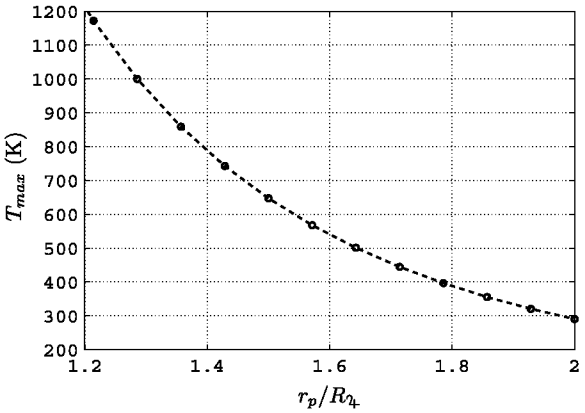

Fig. 8 Maximum temperature as a function of the periapsis of the initial hyperbolic trajectory.

One of the results that can be obtained from Eq. (87) is an estimation of the maximum value of the temperature during the capture. Imposing the condition $\mathrm{d}\mathcal{T}/\mathrm{d}\tau = 0$ yields

$$\mathcal{T}^4_{\max} = 1 + \frac{\sigma_c h_t}{\epsilon_t \sigma_B T_0^4}\left[E_m^2 \frac{(\varphi_C i_C + U_1)}{\ell_1}\right]_{\max} \tag{88}$$

In Fig. 8, the value of $T_{\max} = \mathcal{T}_{\max} T_0$ is shown as a function of the periapsis radius of the initial hyperbolic trajectory, when we suppose the ideal case in the current collection problem, $\varphi_C = 0$, and we consider the attitude is controlled in such a way that $\phi \equiv 0$. The tether is made of aluminum, and its length is 100 km, with the total mass of the system being 3075.5 kg. Note that the mass of the end masses is different from the value of Table 1.

Taking into account that the melting temperature or the aluminum is about 930 K, the periapsis of the initial hyperbolic trajectory should be greater than, say, 1.4 R_J for this particular tether. The measures we can implement to reduce the maximum temperature as well as the current are increasing the value of r_p or reducing the value of L_t or h_t. Because the current is lower along with the maximum temperature, it is more difficult to perform the capture. Additionally, there are other measures that can be taken affecting only the thermal analysis like increasing the value of ϵ_t, decreasing the value of σ_a, or performing the capture in such a way that the periapsis of the trajectory was shadowed by Jupiter (in such a case, $\Psi = 0$ and $\varsigma = \pi/2$), even though these changes would have a minor effect.

VII. Preliminary Operational Limits

According to the previous thermal analysis, it is possible to establish preliminary operational limits of a specific tethered system concerning the maximum allowed temperature of the cable material. That constraint imposes an upper limit on the length of the tether once the other parameters of the system are fixed. On the other hand, to perform a capture, a minimum value of the tether length will be needed. Both restrictions allow to draw the parametric field where the capture can be carried out without reaching too high temperatures.

In Fig. 9, the operational limits for a specific nonrotating tether are shown. The characteristics of the tether are gathered in Table 1. Moreover, a hypothesis has been made concerning the attitude dynamics, assuming that the tether follows the nominal attitude defined in Fig. 3 during the capture. The maximum temperature that is reached during the capture is a function of the periapsis distance and the length of the tether. In Fig. 9, two isothermal lines are plotted, corresponding to 80 and 50% of the melting temperature of the aluminum. The determination of the maximum allowable temperature is complex, given the thermal–mechanical–electrical coupling that exists in this problem. In addition, a line shows the minimum tether length requirement to complete the capture, and two more lines show the required length to obtain final elliptical orbits with periods of 100 and 50 days.

As can be observed, the margin of operation vanishes when the radius of periapsis is close to the radius of Jupiter, and it is broader for larger values of that parameter. Nevertheless, as the radius of periapsis increases, the necessary lengths are also larger.

VIII. Conclusions

A derivation of a method to compute the effect of the electrodynamic forces in the center of mass and attitude dynamics of an electrodynamic tether during a flyby of Jupiter has been carried out in this paper. This method can be applied to other scenarios where low thrust is involved by simply changing the force model (e.g., aerodynamic drag). Nevertheless, it is especially well suited for the case of study in this work due to the great coupling between the attitude and center of mass dynamics.

Using the aforementioned method, numerical simulations of the behavior of the tethered system can be performed easily and accurately to some extent. The results have been compared to those found in the literature and the possibility of a complete capture maneuver by means of only an electrodynamic tether has been corroborated.

Furthermore, a new strategy is proposed to perform the capture: a self-balanced nonrotating electrodynamic tether with the proposed attitude profile. Compared to the option of using a rapidly rotating tethers with a spin pointing in the direction of the magnetic field at the equator, this new proposed technique presents advantages and disadvantages, which are summarized in what follows. The rotating tether concept does not need control to keep its operability and the tension required to maintain the cable straight is provided naturally by the centrifugal force. Nevertheless, it presents also drawbacks because the spin should be obtained by means of thrusters, and the implementation necessary to change the direction of the current each half-revolution is complex. In turn, the nonrotating scheme has a better efficiency and less complexity from the point of view of the

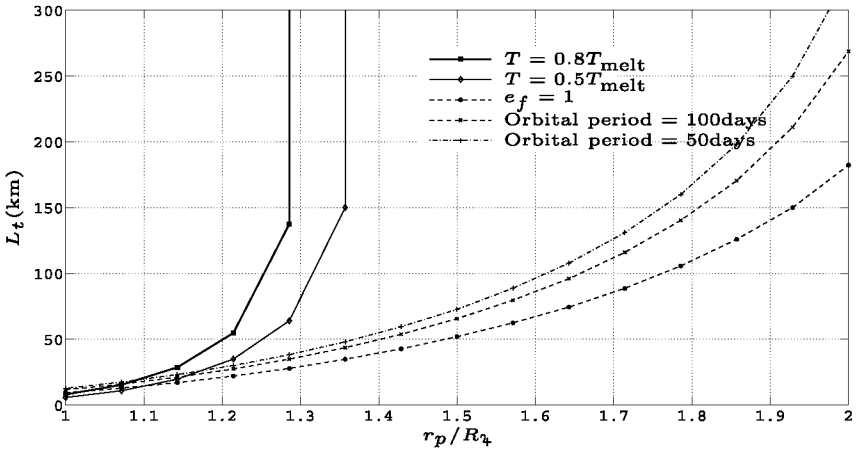

Fig. 9 Operational limits of a tethered system performing a capture at Jupiter.

hardware. However, the control is compulsory, and the needed tension to keep the tether tight considering the lateral forces that act on the cable are not produced passively. The means of generating actively the tension on the cable requires further study and could hamper the viability of this concept.

Finally, preliminary operational limits for the proposed strategy have been provided considering the thermal constraints and the characteristics of the capture. The results show that it is feasible to perform a capture with rigid nonrotating tethers of reasonable characteristics in particular areas of the field of parameters (mainly, hyperbolic initial velocity and radius of periapsis).

Acknowledgments

This work was carried out in the framework of the research project entitled Dynamic simulations of Complex Space Systems (AYA 2010-18796) of the Government of Spain. Propagation of orbits, advanced orbital dynamics, and use of space tethers (ESP2007-64068) was supported by the Dirección General de Investigación (DGI) of the Spanish Ministry of Education and Science.

References

▶[1] Blanc, M., Alibert, Y., Andre, N., Atreya, S., Beebe, R., Benz, W., Bolton, S. J., Coradini, A., Coustenis, A., Dehant, V., Dougherty, M., Drossart, P., Fujimoto, M., Grasset, O., Gurvits, L., Hartogh, P., Hussmann, H., Kasaba, Y., Kivelson, M., Khurana, K., Krupp, N., Louarn, P., Lunine, J., McGrath, M., Mimoun, D., Mousis, O., Oberst, J., Okada, T., Pappalardo, R., Prieto-Ballesteros, O., Prieur, D., Regnier, P., Roos-Serote, M., Sasaki, S., Schubert, G., Sotin, C., Spilker, T., Takahashi, Y., Takashima, T., Tosi, F., Turrini, D., Van Hoolst, T., and Zelenyi, L., "LAPLACE: A Mission to Europa and the Jupiter System for ESA's Cosmic Vision Programme," *Experimental Astronomy*, Vol. 23, No. 3, 2009, pp. 849–892. doi:10.1007/s10686-008-9127-4

[2] Sanmartin, J. R., Charro, M., Bramanti, C., and Bombardelli, C., *Electrodynamic Tether Microsats at the Giant Planets*, European Space Agency, Ariadna Study 05/3203, 2006, Chap. 3.

▶[3] Sanmartin, J. R., Charro, M., Lorenzini, E. C., Garrett, H. B., Bombardelli, C., and Bramanti, C., "Electrodynamic Tether at Jupiter-I: Capture Operation and Constraints," *IEEE Transactions on Plasma Science*, Vol. 36, No. 5, Part 2, Oct. 2008, pp. 2450–2458. doi:10.1109/TPS.2008.2002580

▶[4] Sanmartin, J. R., Charro, M., Lorenzini, E. C., Garrett, H. B., Bombardelli, C., and Bramanti, C., "Electrodynamic Tether at Jupiter-II: Fast Moon Tour After Capture," *IEEE Transactions on Plasma Science*, Vol. 37, No. 4, 2009, pp. 620–626. doi:10.1109/TPS.2009.2013955

▶[5] Charro, M., Sanmartin, J. R., Bombardelli, C., Sanchez-Torres, A., Lorenzini, E. C., Garrett, H. B., and Evans, R. W., "A Proposed Two-Stage Two-Tether Scientific Mission at Jupiter," *IEEE Transactions on Plasma Science*, Vol. 40, No. 2, Part 1, 2012, pp. 274–281. doi:10.1109/TPS.2011.2172637

[6] Peláez, J., and Scheeres, D. J., "On the Control of a Permanent Tethered Observatory at Jupiter," *2007 AAS/AIAA Astrodynamics Specialist Conference*, American Astronomical Society Paper AAS07-369, Aug. 2007.

[7] Peláez, J., and Scheeres, D. J., "A Permanent Tethered Observatory at Jupiter. Dynamical Analysis," *Advances in the Astronautical Sciences*, Vol. 127, 2007, pp. 1307–1330.

▶[8] Bombardelli, C., Lorenzini, E. C., and Sanmartin, J. R., "Jupiter Power Generation with Electrodynamic Tethers at Constant Orbital Energy," *Journal of Propulsion and Power*, Vol. 25, No. 2, 2009, pp. 415–423. doi:10.2514/1.38764

▶[9] Curreli, D., Lorenzini, E. C., Bombardelli, C., Sanjurjo-Rivo, M., Pelaez, J., Scheeres, D., and Lara, M., "Three-Body Dynamics and Self-Powering of an Electrodynamic Tether in a Plasmasphere," *Journal of Propulsion and Power*, Vol. 26, No. 3, 2010, pp. 385–393. doi:10.2514/1.46848

[10] Gallagher, D., Johnson, L., Moore, J., and Bagenal, F., "Electrodynamic Tether Propulsion and Power Generation at Jupiter," NASA TP-1998-208475, 1998.

▶[11] Sanmartín, J., and Lorenzini, E., "Exploration of the Outer Planets Using Tethers for Power and Propulsion," *Journal of Propulsion and Power*, Vol. 21, No. 3, 2005, pp. 573–576. doi:10.2514/1.10772

[12] van Dijk, A., Kruijff, M., van der Heide, E., and Lebreton, J., "LeBRETON—A Lightweight Bare Rotating Tether System for Jovian Atmospheric Entry," *54th International Astronautical Congress of the International Astronautical Federation (IAF)*, International Astronautical Congress Paper IAC-03-S.P.05, Sept.–Oct. 2003.

▶[13] Peláez, J., "Self Balanced Electrodynamic Tethers," *2004 AAS/AIAA Astrodynamics Specialist Conference and Exhibit*, AIAA Paper 2004-5309, Aug. 2004.

▶[14] Peláez, J., and Sanjurjo, M., "Generator Regime of Self Balanced Electrodynamic Tethers," *Journal of Spacecraft and Rockets*, Vol. 43, No. 6, 2006, pp. 1359–1369. doi:10.2514/1.20471

▶[15] Sanmartn, J., Martnez-Sánchez, M., and Ahedo, E., "Bare Wire Anodes for Electrodynamic Tethers," *Journal of Propulsion and Power*, Vol. 9, No. 3, 1993, pp. 353–360.

▶[16] Sanmartn, J., and Estes, R., "The Orbital-Motion-Limited Regime of Cylindrical Langmuir Probes," *Physics of Plasmas*, Vol. 6, No. 1, Jan. 1999, pp. 395–405. doi:10.1063/1.873293

▶[17] Martinez-Sanchez, M., and Sanmartn, J. R., "Artificial Auroral Effects from a Bare Conducting Tether," *Journal of Geophysical Research*, Vol. 102, No. A12, Dec. 1997, pp. 27,257–27,264. doi:10.1029/97JA02044

▶[18] Divine, N., and Garret, H., "Charged Particle Distributions in Jupiter's Magnetosphere," *Journal of Geophysical Research*, Vol. 88, No. A9, 1983, pp. 6889–6903. doi:10.1029/JA088iA09p06889

▶[19] Khurana, K., "Euler Potential Models of Jupiter's Magnetospheric Filed," *Journal of Geophysical Research*, Vol. 102, No. A6, 1997, pp. 11,295–11,306. doi:10.1029/97JA00563

▶[20] Bagenal, F., "Empirical Model of the Io Plasma Torus: Voyager Measurements," *Journal of Geophysical Research*, Vol. 99, No. A6, 1994, pp. 11043–11062. doi:10.1029/93JA02908

[21] Peláez, J., and Sanjurjo-Rivo, M., "Power Generation Using Self-Balanced Electrodynamic Tethers in Debris Mitigation Scenarios," *Advances in the Astronautical Sciences*, Vol. 127, No. 2, 2007, pp. 1409–1426.

▶[22] Scheeres, D. J., Ostro, S. J., Werner, R. A., Asphaug, E., and Hudson, R. S., "Effects of Gravitational Interactions on Asteroid Spin States," *Icarus*, Vol. 147, No. 1, 2000, pp. 106–118. doi:10.1006/icar.2000.6443

▶[23] Scheeres, D. J., "Changes in Rotational Angular Momentum Due to Gravitational Interactions Between Two Finite Bodies," *Celestial Mechanics and Dynamical Astronomy*, Vol. 81, Nos. 1–2, 2001, pp. 39–44.

[24] Cosmo, M., and Lorenzini, E., *Tethers in Space Handbook*, 3rd ed., NASA Rept. NAG8-1160, Dec. 1997.

C. Kluever
Associate Editor